

Nitride Formation and Excess Nitrogen Uptake After Nitriding Ferritic Fe-Ti-Cr Alloys

KYUNG SUB JUNG, SAI RAMUDU MEKA, RALF E. SCHACHERL,
EWALD BISCHOFF, and ERIC J. MITTEMEIJER

The microstructure of the nitrided zone of Fe-Ti-Cr alloys, containing a total of 0.30 at. pct (Ti + Cr) alloying elements, with varying Ti/Cr atomic ratio (0.45, 0.87, and 1.90), was investigated by X-ray diffraction (XRD) and transmission electron microscopy (TEM). The stable TiN and CrN nitrides did not precipitate after nitriding. Instead, ultrafine, metastable, mixed $Ti_{1-x}Cr_xN$ nitride precipitates developed in the nitrided zone: The precipitates were of platelet morphology (length ≤ 30 nm and thickness ≤ 3 nm) and of cubic, rock-salt, crystal-structure type. The misfit strain around the nitride platelets in the ferrite matrix increases with increasing Ti/Cr atomic ratio. As a consequence, most pronouncedly for the highest Ti/Cr atomic ratio, a tetragonally distorted ferrite matrix surrounds the precipitates, as evidenced both by XRD and TEM. The amount of nitrogen taken up was determined quantitatively by measuring the so-called nitrogen-absorption isotherms. It follows that the absorbed amount of so-called excess nitrogen dissolved in the matrix and adsorbed at the nitride-platelet faces increases distinctly with increasing Ti/Cr atomic ratio. The results were discussed in terms of the dependence of misfit strain on the Ti/Cr atomic ratio and the higher chemical affinity of Ti for N than of Cr for N.

DOI: 10.1007/s11661-011-0939-x

© The Minerals, Metals & Materials Society and ASM International 2011

I. INTRODUCTION

NITRIDING is a widely used thermochemical surface treatment for, in particular, ferritic steels.^[1] The formation of inner nitrides can cause a large improvement of the mechanical properties. Because of the possibility of precise control of the nitriding atmosphere, *i.e.*, the chemical potential of nitrogen can be tuned,^[2] gaseous nitriding of metallic alloys, by applying a NH_3/H_2 gas mixture at atmospheric pressure, is often applied to introduce nitrogen in the ferrite matrix at the surface of a specimen. Note that the application of specific NH_3/H_2 gas mixtures allows the adjustment of the chemical potential of nitrogen corresponding hypothetically to thousands of atmospheres of pure N_2 gas.^[3]

During *internal* nitriding of iron-based alloys containing alloying elements (Me) with a strong affinity for nitrogen, as Cr, Al, V, and Ti, fine alloying element nitride precipitates can develop in the nitrided zone

adjacent to the surface (called “diffusion zone”), which leads to a pronounced increase of the hardness of the nitrided component. The increase of hardness and related (mechanical) properties depends strongly on the amount of alloying elements, the chemical composition of the nitride precipitates, the degree of coherency of the nitride precipitates with the matrix, and the precipitate size and morphology.^[4,5]

Until now, most studies concerning internal nitriding have focused on binary Fe-Me alloy systems, *i.e.*, Fe-Cr, Fe-Al, Fe-V, and Fe-Ti.^[6-23] However, commercial nitriding steels often contain more than one alloying element with affinity for nitrogen. Only a few investigations were performed until now on ternary Fe-Me₁-Me₂ alloy systems. Recently, Ti-based ternary nitrides such as (Ti,Al)N, (Ti,Zr)N, and (Ti,Cr)N have gained much attention as second-phase particles in steels because of their contribution to the enhanced performance for cutting tools and machinery components, *e.g.*, regarding wear/corrosion protection.^[24-28]

In the current work, Ti and Cr were selected as alloying elements, because both Cr and Ti, as separate alloying elements, can form nitrides that are cubic (rock-salt crystal structure), albeit of different lattice constants ($a_{CrN} = 4.13\text{\AA}$ and $a_{TiN} = 4.23\text{\AA}$). Cr and Ti have different chemical affinity for nitrogen (Ti has an affinity for N much larger than that of Cr for N). Both TiN and CrN exhibit a Bain orientation relationship ($\{001\}_{bcc, Fe} // \{001\}_{fcc, MeN}$, $\langle 100 \rangle_{bcc, Fe} // \langle 110 \rangle_{fcc, MeN}$) for the nitride precipitates with the ferrite matrix.^[22,23,29-31]

The current project involves investigation of the nitriding behavior of ternary Fe-Ti-Cr alloys. Different Ti/Cr atomic ratios have been employed (Ti/Cr = 0.45, 0.87, and 1.90), while keeping the total amount of

KYUNG SUB JUNG, formerly PhD Student, with the Max Planck Institute for Intelligent Systems (formerly known as Max Planck Institute for Metals Research), Heisenbergstraße 3, 70569 Stuttgart, Germany, is now Senior Research Engineer, with the Samsung Corning Precision Materials, Myeongam-ri, Tangeong-myeon, Chungnam 336-725, South Korea. Contact e-mails: k.s.jung@is.mpg.de and kyungsub98.jung@samsung.com SAI RAMUDU MEKA, PhD Student, and EWALD BISCHOFF, Scientist, are with the Max Planck Institute for Intelligent Systems (formerly known as Max Planck Institute for Metals Research). RALF E. SCHACHERL, Scientist, is with the Institute for Materials Science, University of Stuttgart, Stuttgart 70569, Germany. ERIC J. MITTEMEIJER, Professor, is with the Max Planck Institute for Intelligent Systems (formerly known as Max Planck Institute for Metals Research), and is also with the Institute for Materials Science, University of Stuttgart.

Manuscript submitted November 15, 2010.

Article published online October 27, 2011

alloying element at approximately 0.30 at. pct. The microstructure of the precipitates in the nitrated zone has been investigated by means of X-ray diffraction (XRD) and transmission electron microscopy (TEM). Furthermore, the amount of absorbed nitrogen during nitriding was investigated quantitatively by the analysis of nitrogen-absorption isotherms.

II. EXPERIMENTAL

A. Specimen Preparation

Ingots of Fe-Ti-Cr alloys, containing approximately 0.30 at. pct (Ti + Cr) with varying Ti/Cr atomic ratio (0.45, 0.87, and 1.90), were prepared from pure Fe (99.98 wt pct), pure Ti (99.999 wt pct), and pure Cr (99.999 wt pct) using a light-arc furnace. The molten alloys were cast as buttons, with a shape given by a diameter of 40 mm and a height of 15 mm. The precise composition of the Fe-Ti-Cr alloys was analyzed, applying (1) inductive coupled plasma-optic emission spectroscopy (ICP-OES) to determine the content of the alloying elements Ti and Cr, (2) a combustion method to determine the content of the light elements C and S, and (3) a hot extraction to determine the content of the light elements O and N. The determined composition of the alloys is shown in Table I.

The cast buttons were cold rolled to foils with a thickness of approximately 0.2 mm. To reduce the rolling induced texture of the specimen, specimens of the as-cast buttons were rolled in different directions. From the foils thus obtained, rectangular specimens (15 × 15 mm²) were cut and subsequently ground and polished. The polished specimens were encapsulated in a quartz tube filled with Ar and annealed at 1073 K (800 °C) for 2 hours to establish a recrystallized grain structure (grain size of approximately 30 μm). Before nitriding, the specimens were ground and polished (last step: 1 μm diamond paste) and cleaned ultrasonically with ethanol.

B. Nitriding

For nitriding, the specimens were suspended at a quartz fiber and placed in the middle of a vertical tube furnace. The gaseous nitriding experiments were performed in a flux of ammonia/hydrogen gas mixture (NH₃: >99.998 vol pct and H₂: 99.999 vol pct). The fluxes of both gases were adjusted precisely with mass flow controllers. The gas flow rate was kept at 500 mL/min, which corresponds to a linear gas velocity of 1.35 cm/s in the furnace because the inner diameter of the tube furnace is 28 mm. This value is sufficient to avoid any significant (thermal) decomposition of ammonia in the nitriding atmosphere.^[3]

To maintain a homogeneous precipitation morphology over the entire specimen thickness, during the determination of the absorption isotherms, prenitriding and denitriding steps were performed prior to the nitrogen-absorption isotherm measurements. The prenitriding step involved nitriding at 853 K (580 °C) for 48 hours with a nitriding potential (cf. Reference 3) of $r_N = 0.104 \text{ atm}^{-1/2}$. After completion of this prenitriding, the specimen was quenched into water at room temperature. Subsequently, the specimen was denitrated in a pure H₂ atmosphere at 743 K (470 °C) for 72 hours.

Nitrogen-absorption isotherms were determined at a temperature of 833 K (560 °C) for nitriding potentials r_N in the range from 0.054 atm^{-1/2} to 0.140 atm^{-1/2} (the specimen was nitrided at each nitriding potential for 48 hours; for details, see Table II).

The prenitriding treatment was performed at a nitriding temperature 20 K higher than the temperature applied to record the nitrogen-absorption isotherms. The prenitriding at an increased temperature assures that the precipitation morphology of the specimens does not change during the determination of the nitrogen-absorption isotherms. All applied nitriding treatments in the current work were performed in the α -region of the Lehrer diagram,^[32,33] thus ensuring that no iron nitride formation at the specimen surface occurred.

Table I. Composition of the Cast Alloys, as Determined by Chemical Analysis: Cr and Ti Contents Were Determined by ICP-OES and the Light Element Impurity Contents Were Determined by a Combustion Method for C and S, and by Hot Extraction for O and N

Element	Cr	Ti	Ti/Cr	N	O	S	C
Alloy	(at. pct)			($\mu\text{g/g}$)			
Fe-0.10at. pct Cr-0.19at. pct Ti	0.10 (± 0.01)	0.19 (± 0.02)	1.90	<10	13 \pm 5	<10	9 \pm 2
Fe-0.15at. pct Cr-0.13at. pct Ti	0.15 (± 0.02)	0.13 (± 0.01)	0.87	<10	15 \pm 5	19 \pm 5	7 \pm 2
Fe-0.20at. pct Cr-0.09at. pct Ti	0.20 (± 0.02)	0.09 (± 0.01)	0.45	<10	21 \pm 5	22 \pm 5	6 \pm 2

Table II. Applied Nitriding Parameters for the Pre-nitriding, Denitriding, and Nitriding Experiments for Determination of the Nitrogen-Absorption Isotherms of the Fe-Ti-Cr Alloys

	Temperature [K (°C)]	Time (h)	NH ₃ (mL/min)	H ₂ (mL/min)	r_N (atm ^{-1/2})
Pre-nitriding	853 (580)	48	45	455	0.104
De-nitriding	743 (470)	72	—	500	—
Absorption isotherms	833 (560)	48	58	442	0.140
			50	450	0.117
			40	460	0.091
			25	475	0.054

The amount of nitrogen uptake and/or loss was determined by weight measurements after and before nitriding or denitriding using a Mettler microbalance with an accuracy of 0.1 μg . To obtain an accurate weight value, the average value of ten weight measurements was taken.

C. X-Ray Diffraction

XRD analysis of the specimens before and after nitriding was performed employing a Philips X'Pert diffractometer (PANalytical B.V., Almelo, The Netherlands) in Bragg-Brentano geometry using Co-K_α ($\lambda = 1.7889\text{\AA}$) radiation and a graphite monochromator in the diffracted beam. The measurements were performed in the diffraction-angle, 2θ , range of 40 to 130 deg with a step size of 0.05 deg. The contribution of the Co-K_α radiation of the recorded diffractograms was removed according to Reference 34. The corrected diffractograms were evaluated by fitting a Pearson VII profile-shape function, using TOPAS software (Bruker AXS GmbH, Karlsruhe, Germany), for the diffraction-line profiles in the diffractograms.

D. Microhardness Measurement

Microhardness values before and after nitriding were obtained by conducting hardness measurements across the cross section of specimens employing a Vickers microhardness tester (Leica VMHT Mot). A load of 100 mN, an indenter speed of 30 $\mu\text{m/s}$, and a holding time of 12 seconds for each indentation were applied. The distances between the indentations and the length of both indentation-diagonals were measured with a calibrated light optical microscope (Zeiss Axiophot microscope equipped with Olympus ColorView IIIu digital camera) using analySIS Imaging software. The microhardness values reported in this article are the average of five measurements made at the same depth of the specimen cross section.

E. Transmission Electron Microscopy

Foils for TEM were prepared from the middle of the nitrided zone as follows.

Disks ($\Phi = 3$ mm) were stamped with a mechanical punch from sheets produced by removing material mechanically from both sides (faces) of a nitrided specimen. These disks were thinned to obtain an electron-transparent area, applying the jet-electropolishing technique employing a Struers Tenupol-3 apparatus (bath composition: 85 vol pct acetic acid and 15 vol pct perchloric acid, current: $24 \text{ mA} \leq I \leq 42 \text{ mA}$, voltage: 19.5 V, temperature: 278 K (5 $^\circ\text{C}$), flow rate setting: 20, and treatment time: $174 \text{ seconds} \leq t \leq 242 \text{ seconds}$) and subsequently rinsed in ethanol, acetone and isopropanol. To generate a hole in the middle of the sample, the discs were fixed during the jet-electropolishing treatment between two platinum rings.

A TEM analysis was performed using a Philips CM 200 transmission electron microscope operated at 200 kV. Bright-field (BF) images and selected area diffraction patterns (SADPs) were taken by a Gatan charge-coupled device camera.

F. Electron Probe Microanalysis (EPMA)

To determine the (depth) distribution of the alloying elements and nitrogen after nitriding of the specimens, EPMA was performed on specimen cross sections employing a Cameca SX100 instrument. Pieces of the specimen were cut to prepare cross sections by subsequently embedding of these pieces with a Polyfast (Struers, a conductive bakelite resin with carbon filler embedding material), followed by grinding and polishing (last step: 1 μm diamond paste). A focused electron beam at an accelerating voltage of 15 kV and a current of 100 nA was applied. To obtain the element contents in the specimens, the intensities of the characteristic Ti-K_α , Cr-K_α , Fe-K_β , and N-K_α X-ray emission peaks were determined at points separated at distances of 2 μm along lines perpendicular to the surface of the specimen in the specimen cross section. The concentrations of Ti, Cr, and Fe were determined based on the ratio of the corresponding characteristic X-ray emission peak intensity of the specimen and that of a standard specimen (*i.e.*, pure Ti, pure Cr, and pure Fe) by applying the $\Phi(\rho z)$ -correction.^[35]

For the determination of the characteristic X-ray emission peak of nitrogen, a correction procedure had to be applied because of severe overlap of the N-K_α and Ti-L_1 X-ray emission peaks. The correction procedure, known as the *ratio method*, is as follows^[36]:

- EMPA analysis of the nitrided Fe-Ti-Cr alloy specimen (SPE) provides the intensity $I_{\text{Ti-K}_\alpha}^{\text{SPE}}$ and the total intensity at the 2θ position of the N-K_α emission peak, $I_{\text{tot(N)}}^{\text{SPE}}$, which intensity consists of both $I_{\text{N-K}_\alpha}^{\text{SPE}}$ and a contribution $I_{\text{Ti-L}_1(\text{N})}^{\text{SPE}}$ at the 2θ position of N-K_α .
- The 2θ position and standard intensity of the N-K_α X-ray emission peak are obtained using Fe_4N as a standard material.
- Intensities of the Ti-K_α emission peak ($I_{\text{Ti-K}_\alpha}^{\text{STD}}$ at its own specific 2θ value) and of the Ti-L_1 emission peak at the 2θ position of the N-K_α peak position ($I_{\text{Ti-L}_1(\text{N})}^{\text{STD}}$) are obtained using a pure Ti standard specimen (STD).
- Assuming a constant $\text{Ti-L}_1(\text{N})$ and Ti-K_α intensity ratio for standard (STD) and nitrided specimen (SPE), *i.e.*, ignoring a possible emission peak shift between standard material and the specimen, a correction factor (CF) can be given as follows:

$$\text{CF} = \left(\frac{I_{\text{Ti-L}_1(\text{N})}^{\text{STD}}}{I_{\text{Ti-K}_\alpha}^{\text{STD}}} \right) = \left(\frac{I_{\text{Ti-L}_1(\text{N})}^{\text{SPE}}}{I_{\text{Ti-K}_\alpha}^{\text{SPE}}} \right) \quad [1]$$

- The nitrogen intensity $I_{\text{N-K}_\alpha}^{\text{SPE}}$ can now be calculated from $I_{\text{tot(N)}}^{\text{SPE}}$ and $I_{\text{Ti-K}_\alpha}^{\text{SPE}}$

$$\begin{aligned} I_{\text{N-K}_\alpha}^{\text{SPE}} &= I_{\text{tot(N)}}^{\text{SPE}} - I_{\text{Ti-L}_1(\text{N})}^{\text{SPE}} \\ &= I_{\text{tot(N)}}^{\text{SPE}} \cdot \text{CF} \times \frac{I_{\text{Ti-K}_\alpha}^{\text{SPE}}}{I_{\text{Ti-K}_\alpha}^{\text{SPE}}} \end{aligned} \quad [2]$$

Finally, the concentration of nitrogen is obtained from the ratio of the thus obtained N-K_α intensity of the

specimen and that of the standard material (γ -Fe₄N), applying the $\Phi(\rho z)$ approach (see preceding section).

III. RESULTS AND EVALUATION

A. The Nitrided Microstructure

X-ray diffractograms were taken from the specimen surface before and after nitriding for all Fe-Ti-Cr alloys (Ti/Cr atomic ratio = 0.45, 0.87, and 1.90). Only ferrite reflections appear in the diffractograms. For all alloys, the diffraction peaks of the ferrite, particularly the $200_{\alpha\text{-Fe}}$ reflection, had broadened strongly after nitriding (Figures 1(a) through (c)). The occurrence of pronounced diffraction-line broadening of the ferrite reflexes after nitriding, without the appearance of separate alloying element nitride reflections, can be ascribed to the development of microstrain because of the formation of (largely) coherent precipitates in the ferrite matrix, which diffract coherently with the matrix, as discussed in Reference 37. In addition to the observed

broadening of the $200_{\alpha\text{-Fe}}$ diffraction line, an intensity hump arises at the high-angle side of the $200_{\alpha\text{-Fe}}$ reflection. It becomes more pronounced with increasing Ti/Cr atomic ratio of the specimen (see, especially, the intensity data within the dashed circle in Figure 1(d)).

TEM BF and corresponding SADPs of nitrided Fe-Ti-Cr alloys with Ti/Cr = 0.45 and 1.90 are shown in Figures 2(a) and (b), respectively. The electron-beam direction in both SADPs is close to (*i.e.*, does not coincide exactly with) the [001] zone axis of the ferrite to avoid strong diffraction by the matrix and to reveal the presence of the precipitates by their diffraction contrast. The TEM BF diffraction-contrast images show an ultra-thin platelet morphology of the nitride precipitates in the ferrite matrix (see the dotted circles in the BF images, which indicate regions showing the typical coffee-bean contrast resulting from the misfit strain between the thin nitride platelets and the ferrite matrix for platelets parallel to the [001]_{α-Fe} electron beam/zone axis. The nitride platelets in the dotted circles are parallel to (100)_{α-Fe} matrix lattice planes (see subsequent

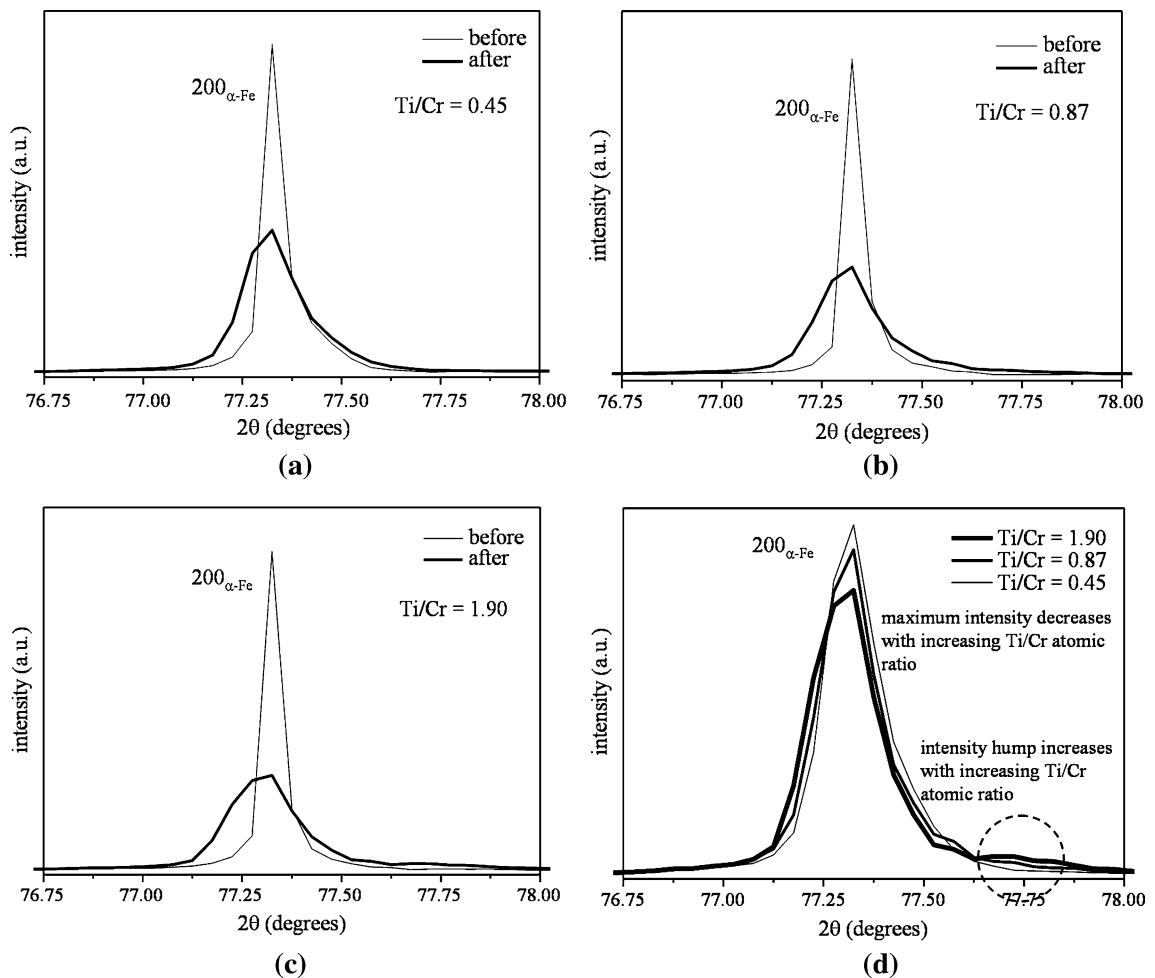


Fig. 1—X-ray diffractograms of the $200_{\alpha\text{-Fe}}$ reflection ($76.5 \text{ deg} < 2\theta < 78.5 \text{ deg}$, Co-K α radiation, step size 0.05 deg; normalized with respect to the integral intensity) before and after nitriding of the Fe-Ti-Cr alloy concerned. (a) Ti/Cr = 0.45, (b) Ti/Cr = 0.87, (c) Ti/Cr = 1.90, and (d) composite of all $200_{\alpha\text{-Fe}}$ reflections (a–c) after nitriding. The nitriding experiments were performed at 853 K (580 °C) for 48 h with nitriding potential $r_N = 0.104 \text{ atm}^{-1/2}$.

section). The size of the platelets (length $\leq 30\text{nm}$ and thickness $\leq 3\text{nm}$) does not depend significantly on the Ti/Cr atomic ratio.

The SADPs show pronounced streaks through the $200_{\alpha\text{-Fe}}$ diffraction spots in the $\langle 100 \rangle_{\alpha\text{-Fe}}$ directions and additional diffraction spots near the $110_{\alpha\text{-Fe}}$ diffraction spots corresponding with a lattice spacing d , which is compatible with the spacing of the $\{111\}$ lattice planes of a cubic, rock-salt, structure-type nitride (MeN). Moreover, particularly for the highest Ti/Cr ratio (see SADP in Figure 2(b)), the $200_{\alpha\text{-Fe}}$ diffraction spots have split into two: one corresponding to cubic ferrite (d_{200} of cubic ferrite from SADP = 1.43\AA) and another one corresponding to tetragonally distorted ferrite.

The intensity hump observed in the X-ray diffractograms at the high-angle side of the $200_{\alpha\text{-Fe}}$ reflection (see dashed circle in Figure 1(d)) is compatible with the occurrence of a split $200_{\alpha\text{-Fe}}$ spot in the SADP shown in Figure 2(b). As demonstrated here by fitting (using a Pearson VII profile-shape function) to the overall $200_{\alpha\text{-Fe}}$ reflection shown in Figure 1(c), the overall reflection is composed of two peaks (see Figure 3 for the nitrated Fe-Ti-Cr alloy with Ti/Cr = 1.90): one is ascribed to a

cubic ferrite 200 reflection (d_{200} of cubic ferrite = 1.43\AA) and the other one is ascribed to the $200/002$ doublet reflection of tetragonally distorted ferrite (d_{200} of tetragonal ferrite = 1.43\AA and d_{002} of tetragonal ferrite = 1.42\AA). The fit of the tetragonal doublet and cubic reflections to the measured intensity data, as shown in Figure 3, was performed adopting the procedure described in Reference 37 (note that in Reference 37, the c and a lattice parameters of the body-centered tetragonal (bct) phase have been, unconventionally, defined such that $c = b$ instead of $a = b$). These d spacings, derived from the XRD pattern, are compatible with the split $200_{\alpha\text{-Fe}}$ diffraction spot in the SADP shown in Figure 2(b).

The positions in the SADPs of the 111_{MeN} diffraction spots, near the $110_{\alpha\text{-Fe}}$ diffraction spots and ascribed to the face-centered cubic (fcc), rock-salt type MeN structure, are compatible with the occurrence of a Bain orientation relationship of cubic, rock-salt, structure-type MeN precipitates with the bcc ferrite matrix: $\{001\}_{\text{bcc}} // \{001\}_{\text{fcc}}$, $\langle 100 \rangle_{\text{bcc}} // \langle 110 \rangle_{\text{fcc}}$ (cf. References 37 and 38).

The nitride platelets develop with $\{001\}_{\alpha\text{-Fe}}$ lattice planes as habit planes. The mismatch of the nitride

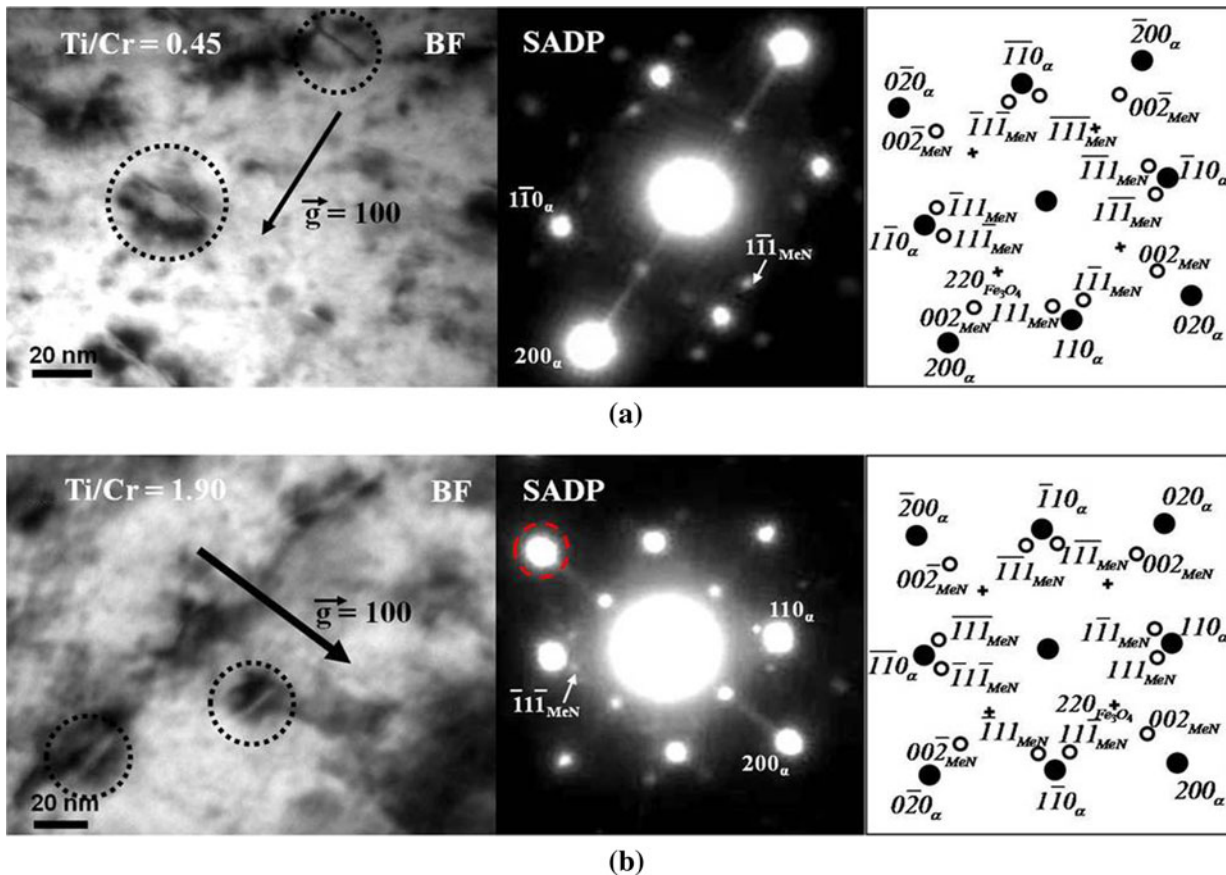


Fig. 2—TEM BF images (left) showing diffraction contrast resulting from fine (misfitting) $\text{Ti}_{1-x}\text{Cr}_x\text{N}$ nitride platelets in the ferrite matrix. (a) Ti/Cr = 0.45 and (b) Ti/Cr = 1.90. The dotted open circles in the BF images indicate locations where fine nitride platelets had developed, giving rise to misfit strain field induced “coffee-bean” contrast. The SADPs (middle) were taken at electron-beam directions close to $[001]_{\alpha\text{-Fe}}$. The SADP of the Fe-Ti-Cr, Ti/Cr = 1.90 alloy in (b) shows elongated $200_{\alpha\text{-Fe}}$ diffraction spots (see dashed circle), which is composed of a cubic ferrite 200 diffraction spot and a 200 diffraction spot originating from tetragonally strained ferrite (see text). Schematic diffraction patterns (right), corresponding with the SADPs shown, for the concerned electron-beam, *i.e.*, $[001]_{\alpha\text{-Fe}}$ direction and nitride precipitates complying with a Bain orientation relationship with the $\alpha\text{-Fe}$ matrix (black dots: diffraction spots of the ferrite matrix; unfilled circles: diffraction spots of the nitride precipitates).

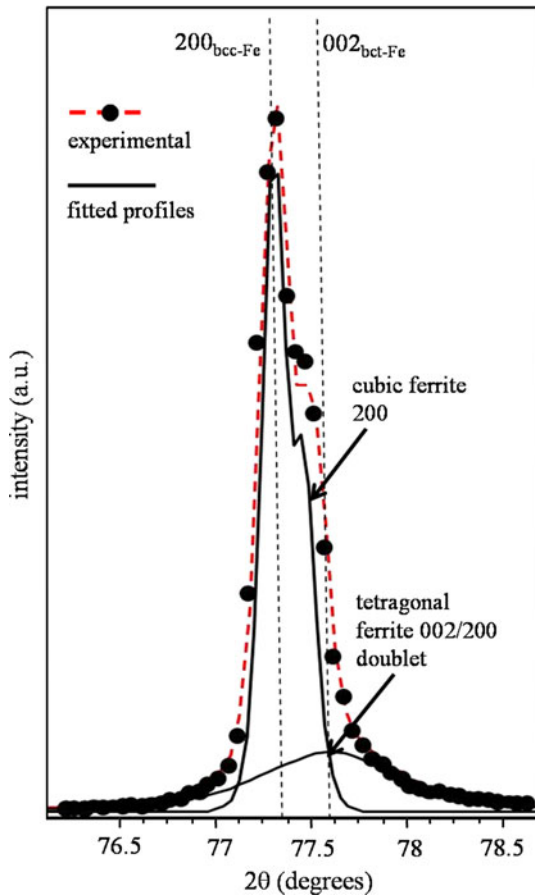


Fig. 3—Contributions of the 200 reflection of the (cubic, bcc) ferrite and the 200/002 doublet reflection of the tetragonally distorted (bct) ferrite to the total observed diffraction profile as evaluated by fitting a Pearson VII profile-shape function for the various reflection contributions (Ti/Cr = 1.90).

platelet with the ferrite matrix is such that, to maintain coherency, the ferrite matrix in the immediate surroundings of the nitride platelets is anisotropically, tetragonally deformed: A compressive misfit stress develops in the directions normal to the platelet (*i.e.*, in a $\langle 001 \rangle_{\alpha\text{-Fe}}$ direction), whereas a tensile misfit stress develops parallel to the platelet faces (*i.e.*, in $\langle 100/010 \rangle_{\alpha\text{-Fe}}$ directions). The surrounding ferrite matrix of the nitride platelet can thus be considered as a bct phase (see Figure 4).

If precipitates of CrN and TiN would have developed separately in the ferrite matrix during nitriding, the diffraction spots of both nitrides should be distinguishable (in the SADPs). However, the SADPs show only singular 111 reflections of a cubic, rock-salt, crystal-structure type MeN nitride. This finding suggests that Ti and Cr have precipitated together in a cubic, rock-salt type mixed $\text{Ti}_{1-x}\text{Cr}_x\text{N}$ nitride (such mixed precipitation, leading to a metastable precipitate, $(\text{Me}_1, \text{Me}_2)\text{N}$, in principle prone to decomposition into the two equilibrium precipitates, Me_1N and Me_2N , was observed for the first time after nitriding Fe-Cr-Al alloys^[38]). The d spacing measured from the 111 reflection of the mixed $\text{Ti}_{1-x}\text{Cr}_x\text{N}$ (Ti/Cr = 0.45) is 2.41 Å, which (indeed) is in between the 111 d spacing of CrN (2.38 Å) and the 111 d

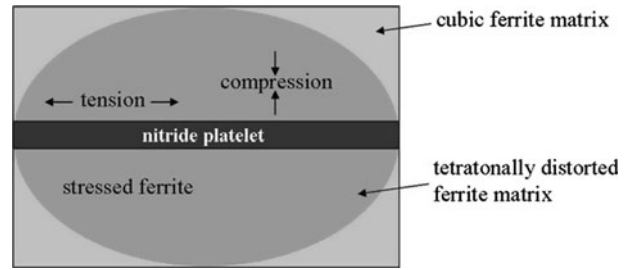


Fig. 4—Schematic presentation of a misfitting coherent nitride platelet and the surrounding ferrite matrix, and the associated state of stress in the matrix.

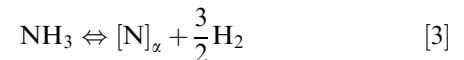
spacing of TiN (2.44 Å). Furthermore, the lattice parameter derived from the 111 reflection of mixed $\text{Ti}_{1-x}\text{Cr}_x\text{N}$ with Ti/Cr = 0.45 (see previous section), which is 4.17 Å, agrees well with that reported for a (Ti, Cr)N (Ti/Cr = 0.45) film produced by reactive cathodic sputtering.^[39,40]

The lattice parameters of mixed $\text{Ti}_{1-x}\text{Cr}_x\text{N}$ nitride, as derived from the reflections recorded in the SADPs, are shown as function of the relative Ti content in Figure 5, together with those pertaining to pure CrN and pure TiN. Evidently, the lattice parameter of mixed $\text{Ti}_{1-x}\text{Cr}_x\text{N}$ nitride increases linearly with increasing relative Ti content, indicating that the substitutional solid solution of Ti and Cr in the mixed nitride complies with Vegard's law. This provides additional support for the previous interpretation implying that mixed $\text{Ti}_{1-x}\text{Cr}_x\text{N}$ nitride forms after nitriding.

B. Quantitative Analysis of Excess Nitrogen Uptake

A nitrogen-absorption isotherm shows the dependence of the amount of nitrogen taken up by a (homogeneously) nitrated specimen as function of the nitriding potential, r_N (directly related to the chemical potential of nitrogen absorbed in the ferrite matrix for a given nitriding atmosphere^[2]). The analysis of nitrogen-absorption isotherms allows distinction of various kinds of differently (chemically) bonded nitrogen.

The amount of nitrogen absorbed in the ferrite matrix after nitriding by means of an NH_3/H_2 gas mixture can be described by the equilibrium



where $[\text{N}]_x$ is the concentration of nitrogen dissolved interstitially in the ferrite matrix. The solubility of nitrogen in ferrite matrix $[\text{N}]_x$ is proportional to the nitriding potential, r_N ($= \frac{p_{\text{NH}_3}^{1/2}}{p_{\text{H}_2}}$, with p as partial pressure), according to

$$[\text{N}]_x = K \cdot r_N \quad [4]$$

where K is the equilibrium constant for Eq. [3] and it has been assumed that the activity coefficient of the nitrogen atoms is constant and has been incorporated in K .^[2]

Any point on a nitrogen-absorption isotherm indicates the equilibrium amount of nitrogen absorbed by

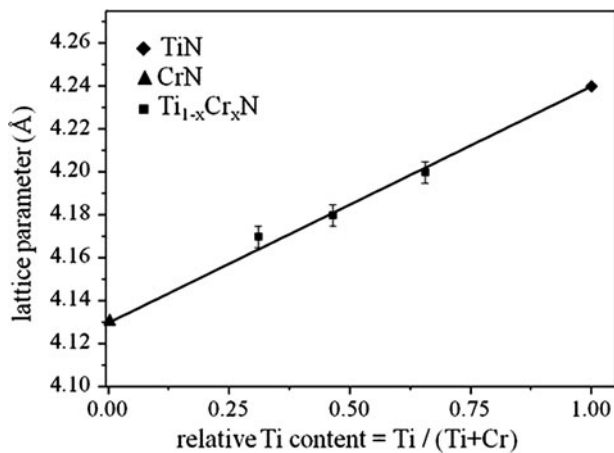


Fig. 5—Lattice parameters of pure CrN (open triangle), pure TiN (open diamond), and mixed $Ti_{1-x}Cr_xN$ (open squares) as a function of relative Ti atomic content (relative with respect to the total amount of alloying elements, *i.e.*, Ti + Cr).

the specimen at a given nitriding potential. To determine experimentally nitrogen-absorption isotherms, it is essential to establish a homogeneous, constant nitrogen content throughout the cross-section of the specimen. Furthermore, the precipitation morphology should not change during determination of the absorption isotherm. Therefore, the preceding prenitriding treatment (cf. Section II-B) is performed at a temperature higher than applied for determination of the absorption isotherm, to ensure a constant precipitate morphology. It has been verified that such conditions have been realized in the current work.

Elemental concentration-depth profiles determined for the entire cross section of the specimens (pre)nitrided at 853 K (580 °C) for 48 hours (EPMA data) are shown in Figures 6(a) through (c) for the alloys with Ti/Cr = 0.45, 0.87, and 1.90, respectively. Evidently, after the homogeneous nitriding, the nitrogen uptake is greater than the amount of nitrogen required for the precipitation of all Ti and Cr as mixed $Ti_{1-x}Cr_xN$ nitride $[N]_{Ti_{1-x}Cr_xN}$, plus the amount of nitrogen necessary to establish the equilibrium solubility in an unstrained ferrite matrix, $[N]_z^0$. This so-called amount of “normal” nitrogen, $[N]_{nor} \equiv [N]_{Ti_{1-x}Cr_xN} + [N]_z^0$, has been indicated by the horizontal-dashed line in Figures 6(a) through (c). The difference between the experimentally obtained total amount of nitrogen, $[N]_{tot}$, and the amount of “normal” nitrogen, $[N]_{nor}$, is defined as excess nitrogen, $[N]_{ex}$ (for details see References 18 and 31).

After prenitriding, the specimens were subsequently denitrided in a pure H_2 (500 mL/min) atmosphere at 743 K (470 °C) for 72 hours. After the denitriding step, the nitrogen content that remains in the specimen was determined by weighing. The remaining nitrogen content in the Fe-Ti-Cr alloys amounts to 0.25 (± 0.04), 0.25 (± 0.01), and 0.26 (± 0.01) at. pct* for the alloys with

Ti/Cr = 0.45, 0.87 and 1.90, respectively, which can be fully attributed to nitrogen strongly bonded to Ti and Cr in corresponding nitride precipitates $Ti_{1-x}Cr_xN$. This indicates that all excess nitrogen was removed from the specimens by the denitriding treatment.

The nitrogen-absorption isotherms for each specimen (after prenitriding and denitriding, as discussed) are shown in Figures 7(a) through (c) for the alloys with Ti/Cr = 0.45, 0.87, and 1.90, respectively. A straight line (dashed line in Figures 7(a) through (c)) can be fitted (least squares analysis) to the data points representing the total amount of absorbed nitrogen. The extrapolation to $r_N = 0$ yields the data point *A* on the ordinate as shown in Figures 7(a) through (c). The nitrogen level indicated with *B* on the ordinate in Figures 7(a) through (c) represents the amount of nitrogen required for the formation of stoichiometric mixed $Ti_{1-x}Cr_xN$ nitride precipitates (*i.e.*, $[N]_{Ti_{1-x}Cr_xN}$), that is, the (measured) amount of nitrogen remaining after denitriding (see previous section). Hence, in line with the reasoning applied for, *e.g.*, Fe-V^[19] and Fe-Cr^[6] alloys, it is suggested that the difference $A - B$ can be ascribed to (excess) nitrogen adsorbed at the interface between nitride precipitate and ferrite matrix, $[N]_{interface}$. The thus obtained $[N]_{interface}$ values have been gathered, together with the values of levels *A* and *B*, in Table III and Figure 8(a).

The composition of a $Ti_{1-x}Cr_xN$ precipitate together with the interfacial adsorbed excess nitrogen $[N]_{interface}$ can be described as $Ti_{1-x}Cr_xN_y$, where

$$y = \frac{[N]_{Ti_{1-x}Cr_xN} + [N]_{interface}}{[N]_{Ti_{1-x}Cr_xN}} = \frac{\text{level } A}{\text{level } B} \quad [5]$$

The value of y thus obtained contains indirect information on the average thickness of the precipitate platelet. As shown in Section III-A, $Ti_{1-x}Cr_xN$ precipitates develop as platelets of a cubic, rock-salt, crystal-structure type obeying a Bain orientation relationship with the ferrite matrix. With $\{001\}_{Ti_{1-x}Cr_xN}$ as a habit plane, the thickness of a monolayer of $Ti_{1-x}Cr_xN$ is $\frac{1}{2}$ the lattice parameter of the rock-salt, crystal-structure type (*i.e.*, $\frac{a_{Ti_{1-x}Cr_xN}}{2}$). If at every octahedral interstice in the ferrite matrix at the nitride/matrix interface one excess nitrogen atom is trapped, it follows

$$y = \frac{n + 2}{n} \quad [6]$$

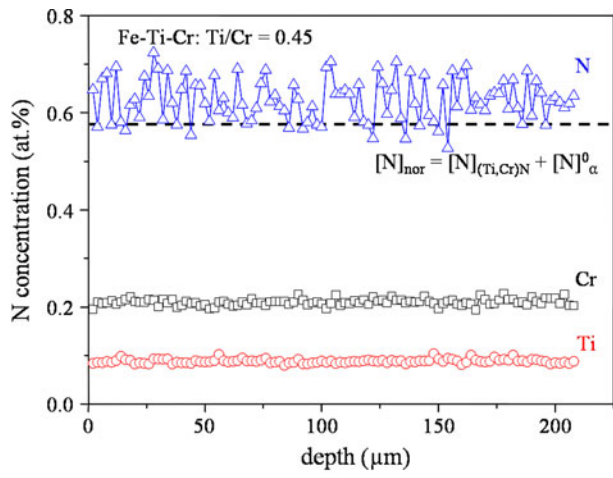
where n is the number of $Ti_{1-x}Cr_xN$ monolayers comprising the platelet. Thus, the thickness t of a $Ti_{1-x}Cr_xN$ platelet follows from

$$t = n \cdot \frac{a_{Ti_{1-x}Cr_xN}}{2} = \frac{a_{Ti_{1-x}Cr_xN}}{y - 1} \quad [7]$$

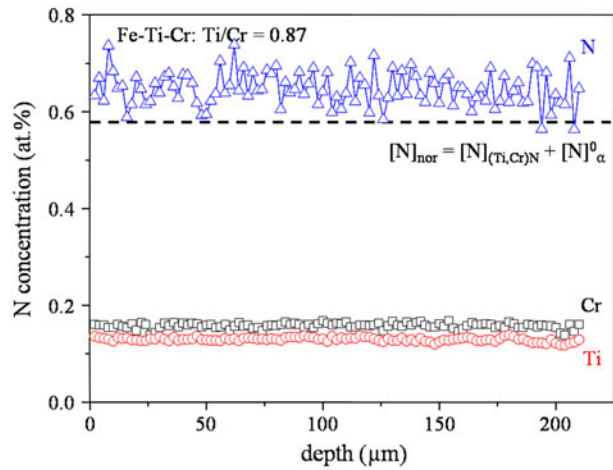
Using lattice-parameter data of mixed $Ti_{1-x}Cr_xN$ nitride as obtained in this work (Figure 5), the obtained nitride-platelet thickness values have been gathered in Table IV together with the corresponding y values.

These deduced thickness values obtained are compatible with the data obtained by the TEM investigations (Section III-A).

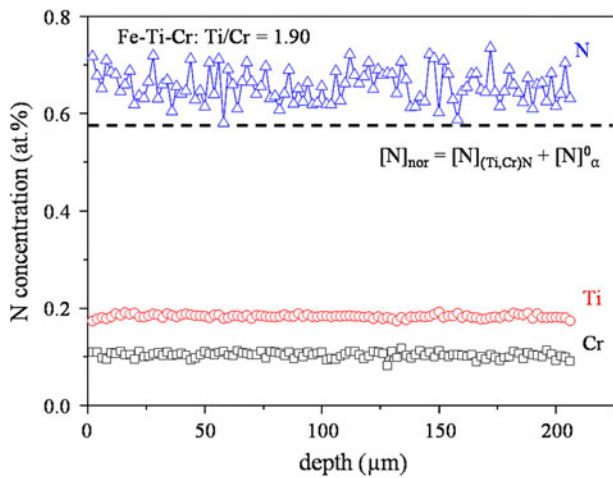
*The error ranges indicated were taken equal to the *maximal* deviation from the average value calculated on the basis of the ten weight measurements before and after (de)nitriding.



(a)

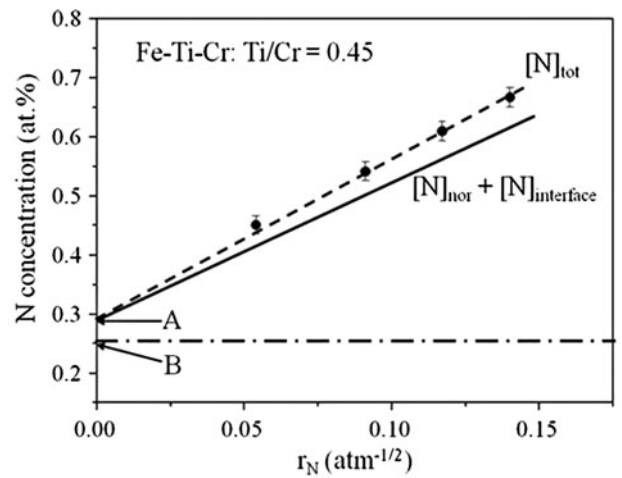


(b)

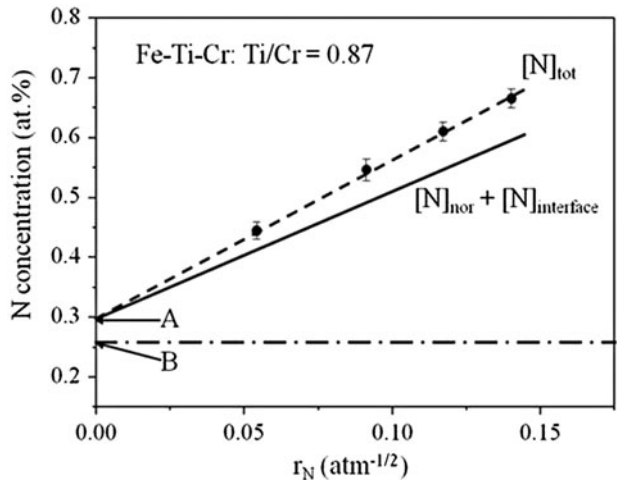


(c)

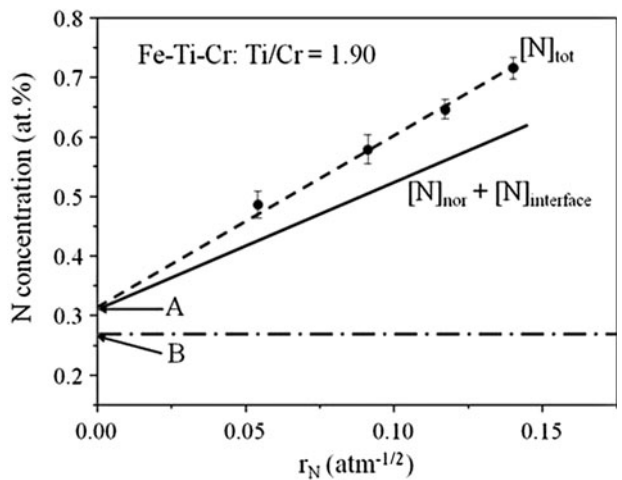
Fig. 6—N, Ti, and Cr (EPMA) concentration-depth profiles measured for the entire cross sections of nitrated Fe-Ti-Cr specimens. (a) Ti/Cr = 0.45, (b) Ti/Cr = 0.87, and (c) Ti/Cr = 1.90 after prenitriding [48 h at 853 K (580 °C) with $r_N = 0.104 \text{ atm}^{-1/2}$]. The dashed horizontal line denotes the amount of “normal” nitrogen, which is the sum of the amounts of nitrogen necessary to transform all alloying elements into alloying element nitrides $[N]_{\text{Ti},\text{Cr},\text{N}}$ and of nitrogen dissolved interstitially in the unstrained ferrite matrix $[N]_{\alpha}^0$.



(a)



(b)



(c)

Fig. 7—Nitrogen-absorption isotherms after successive prenitriding and denitriding treatments for Fe-Ti-Cr alloys (a) Ti/Cr = 0.45, (b) Ti/Cr = 0.87, and (c) Ti/Cr = 1.90. The linear portions of the nitrogen-absorption isotherms have been indicated by the dashed lines that intersect the ordinates at $r_N = 0$ at nitrogen levels indicated by A. The nitrogen levels after denitriding (horizontal dash-dot lines) have been indicated by B.

Table III. The Values of Nitrogen Uptake at Level A (Interception of the Dashed Line in Figs. 7(a) through (c) with the Ordinate, *i.e.*, at Nitriding Potential, $r_N = 0$), at Level B (as Obtained after Denitriding), and the Accordingly Calculated Amount of Nitrogen Adsorbed at the Interface Nitride Precipitate/Ferrite Matrix, $[N]_{\text{interface}}$ (*i.e.*, $A-B$)

Alloy	A (at. pct)	B (at. pct)	$[N]_{\text{interface}}$ (at. pct)
Fe-Ti-Cr: Ti/Cr = 0.45	0.290	0.251 (± 0.015)	0.039 (± 0.015)
Fe-Ti-Cr: Ti/Cr = 0.87	0.296	0.254 (± 0.014)	0.042 (± 0.014)
Fe-Ti-Cr: Ti/Cr = 1.90	0.311	0.260 (± 0.013)	0.051 (± 0.013)

As follows from Eq. [4], $[N]_{\alpha} = [N]_{\text{tot}} - A$ represents the amount of nitrogen dissolved in the ferrite matrix. The normal amount of dissolved nitrogen $[N]_{\alpha}^0$ is represented by $[N]_{\alpha}^0 = [N]_{\text{nor}} + [N]_{\text{interface}} - A$; see the full line indicated with $[N]_{\text{nor}} + [N]_{\text{interface}}$ in Figures 7(a) through (c). The difference between the dashed and full straight lines represents the excess nitrogen dissolved in the ferrite matrix. This dissolved excess nitrogen $[N]_{\text{strain}}$ is caused by the presence of strain fields around the misfitting nitride precipitates.^[31] Positive volumetric misfit is associated with the precipitation of nitride precipitates in the ferrite matrix. Assuming fully elastic accommodation of this misfit, a finite matrix shows positive lattice dilation. The matrix-lattice dilation generated by the misfitting nitrides, induced by the hydrostatic component of the image-stress field of finite bodies, provides a geometrical understanding for the occurrence of an enhanced amount of dissolved nitrogen.

From the slope of the extrapolated straight dashed line S , the amount of $[N]_{\text{strain}}$ can be calculated:

$$S = \frac{\Delta[N]_{\alpha}}{\Delta r_N} = \frac{\Delta[N]_{\alpha}^0 + \Delta[N]_{\text{strain}}}{\Delta r_N} = S_{\alpha}^0 + \frac{\Delta[N]_{\text{strain}}}{\Delta r_N} \quad [8]$$

The value of S_{α}^0 at a given nitriding temperature can be obtained from the nitriding behavior of pure α -Fe (such data used here have been taken from Reference 41). Hence, from the slope S the value of $[N]_{\text{strain}}$ can be given as fraction of r_N (Figure 8(b)). It follows that $[N]_{\text{strain}}$ increases distinctly with increasing Ti/Cr atomic ratio. This suggests that the level of microstrain in the ferrite matrix increases with increasing Ti/Cr atomic ratio.

This result is compatible with the measured microhardness data: the average microhardness of the specimens before and after nitriding is shown in Figure 9 as a function of the Ti/Cr atomic ratio. The hardness of the nitrided specimen increases significantly with increasing Ti/Cr ratio. This result is compatible with the X-ray diffraction data, which indicate an increase of microstrain level with increasing Ti/Cr atomic ratio (see the XRD results and their discussion in Section III-A).

The total amount of excess nitrogen is given by the sum of $[N]_{\text{strain}}$ (dependent on r_N) and $[N]_{\text{interface}}$ (independent of r_N): $[N]_{\text{excess}} = [N]_{\text{strain}} + [N]_{\text{interface}}$. Evidently, as $[N]_{\text{strain}}$, $[N]_{\text{interface}}$ also increases with increasing Ti/Cr atomic ratio (cf. Figure 8).

IV. GENERAL DISCUSSION: THE ROLE OF THE Ti/Cr ATOMIC RATIO

During nitriding of ferritic ternary Fe-Ti-Cr alloys, a cubic, rock-salt, crystal-structure type, mixed $\text{Ti}_{1-x}\text{Cr}_x\text{N}$

nitride platelets precipitates. The chemical affinity of Ti for N to precipitate as TiN is much larger than that of Cr for N to precipitate as CrN.^[31] This suggests a much larger driving force for Ti than for Cr to precipitate as nitride after nitriding. There is no difficulty for the mixed nitride to form the cubic, rock-salt, crystal-structure type: Both TiN and CrN have this crystal structure. In particularly considering the misfit-strain development on formation of nitride precipitates in the ferrite matrix, it follows that uptake of Cr in TiN can be favored because it leads to reduction of the misfit strain with the surrounding ferrite matrix (see subsequent text). It can be suggested that the Cr atoms are “dragged” into the developing cubic, rock-salt, structure-type TiN precipitates, thereby forming mixed $\text{Ti}_{1-x}\text{Cr}_x\text{N}$ nitride.

The mixed $\text{Ti}_{1-x}\text{Cr}_x\text{N}$ nitride platelets exhibit a Bain orientation relationship with the ferrite matrix with $\{001\}_{\alpha\text{-Fe}}$ habit planes parallel to the platelet faces. The platelet morphology is a consequence of the strongly anisotropic misfit strain with the surrounding ferrite matrix: The linear misfits of the mixed $\text{Ti}_{1-x}\text{Cr}_x\text{N}$ nitride platelet (Ti/Cr = 0.45) along and perpendicular to the $\{001\}_{\alpha\text{-Fe}}$ habit planes are approximately 3.8 pct and 47 pct, respectively. This anisotropic nature of the misfit strain field, together with the coherent nature of the interface between nitride platelets and ferrite matrix, induces the tetragonal distortion of the ferrite matrix adjacent to the nitride platelets (Figure 4).

The lattice parameter of mixed $\text{Ti}_{1-x}\text{Cr}_x\text{N}$ nitride increases with increasing Ti/Cr atomic ratio (cf. Figure 5). In view of the Bain orientation relationship and the lattice parameter of pure α -Fe, this implies that the misfit-strain field surrounding the precipitates becomes more pronounced with the increasing atomic Ti/Cr ratio. As a consequence, a significant hardness increase occurs with increasing atomic Ti/Cr ratio (the minor differences in the total amounts of nitrogen dissolved in the ferrite matrix (cf. data for $[N]_{\text{tot}} - A$ in Figure 7) cannot cause this effect; see also Figure 4 in Reference 42). Indeed, the diffraction-line broadening observed for the ferrite matrix and the tetragonal distortion of the ferrite matrix as revealed by the intensity hump at the high-angle side of the $200_{\alpha\text{-Fe}}$ reflection increase with increasing Ti/Cr atomic ratio (cf. Figure 1(d)).

The coherent nature of the nitride platelet/matrix interface makes adsorption of nitrogen at the octahedral interstices in the ferrite matrix *adjacent* to the platelet faces likely, as in this way bonding to Ti and/or Cr in the platelet is realized, *i.e.*, $[N]_{\text{interface}}$. Because the affinity of Ti for N is much higher than that of Cr for N, $[N]_{\text{interface}}$ increases with Ti/Cr, as observed (Figure 8(a)). A similar

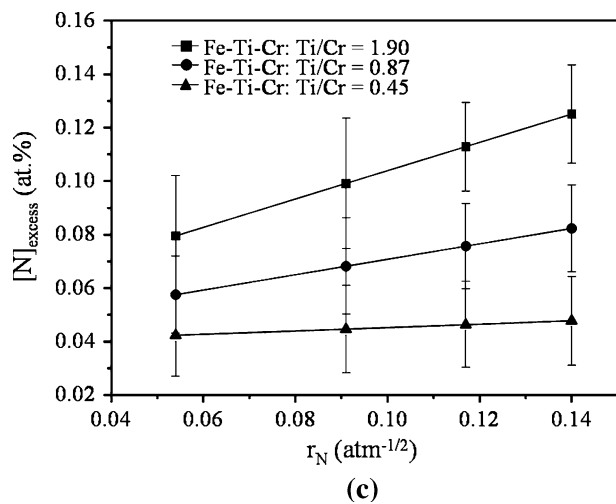
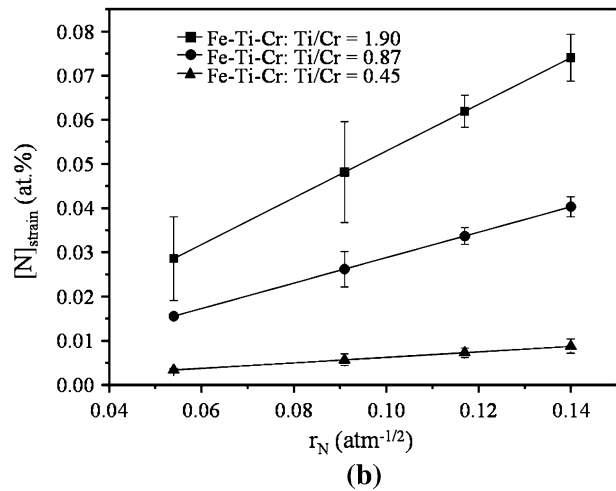
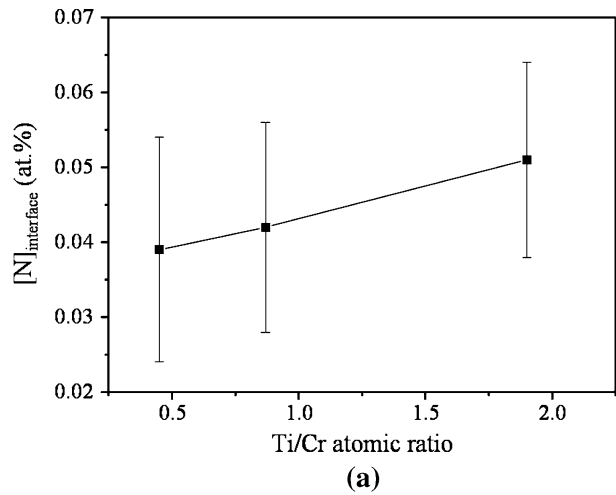


Fig. 8—Excess nitrogen (a) adsorbed at the nitride precipitates/ferrite matrix interface, $[N]_{\text{interface}}$, as a function of Ti/Cr atomic ratio (b) dissolved interstitially in the ferrite matrix because of the presence of a misfit-strain field, $[N]_{\text{strain}}$, and (c) total amount of excess nitrogen ($= [N]_{\text{interface}} + [N]_{\text{strain}}$) for Fe-Ti-Cr alloys (Ti/Cr = 0.45, 0.87, and 1.90) as function of the nitriding potential r_N .

observation was made for nitrided Fe-Cr-Al alloys where $[N]_{\text{interface}}$ increases with increasing Al/Cr atomic ratio.^[41–43] Moreover, for increasing Ti/Cr atomic ratio,

Table IV. The Value of y in $\text{Ti}_{1-x}\text{Cr}_x\text{N}_y$, and the Accordingly Deduced (See Text) Average Thickness of the $\text{Ti}_{1-x}\text{Cr}_x\text{N}$ Platelets (Calculated Using Eq. (6)) for Fe-Ti-Cr Alloys With Atomic Ratio Ti/Cr = 0.45, 0.87, and 1.90

Alloy	y in $\text{Ti}_{1-x}\text{Cr}_x\text{N}_y$	Average Thickness of Platelets (nm)
Fe-Ti-Cr: Ti/Cr = 0.45	1.16	2.6
Fe-Ti-Cr: Ti/Cr = 0.87	1.18	2.3
Fe-Ti-Cr: Ti/Cr = 1.90	1.20	2.1

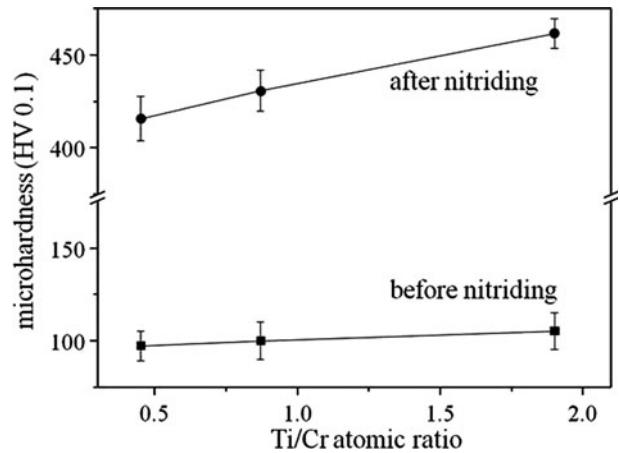


Fig. 9—Microhardness of the Fe-Ti-Cr alloys (Ti/Cr = 0.45, 0.87, and 1.90) before and after nitriding as a function of their Ti/Cr atomic ratio. The error ranges indicated were taken equal to the maximal deviation from the average value (10 measurements) for each data point.

the nitride-platelet thickness decreases (Table IV), implying that the amount of interfacial area between nitride precipitates and the matrix increases with an increasing Ti/Cr atomic ratio. Obviously, this effect contributes to an increase of $[N]_{\text{interface}}$ with increasing Ti/Cr atomic ratio, as well.

The presence of dissolved excess nitrogen in the ferrite matrix after nitriding of the Fe-Ti-Cr alloys is a consequence of elastic accommodation of the misfit between nitride platelet and ferrite matrix: Such elastic accommodation of misfit induces a tensile hydrostatic stress component in the ferrite matrix.^[31] As a consequence, compared with the unstrained state, more nitrogen can be dissolved (on octahedral interstices) in the ferrite matrix; *i.e.*, $[N]_{\text{strain}}$. Because the misfit increases with increasing Ti/Cr atomic ratio, $[N]_{\text{strain}}$ increases with increasing Ti/Cr atomic ratio, as observed (Figure 8(b)).

V. CONCLUSIONS

1. After nitriding of ternary iron-based Fe-Ti-Cr alloys highly coherent cubic, rock-salt, crystal-structure type, mixed $\text{Ti}_{1-x}\text{Cr}_x\text{N}$ nitrides develop in the ferrite matrix. Separate TiN and CrN nitrides do not develop. The uptake of Cr in TiN is favored as it reduces the misfit-strain field in the ferrite matrix.

2. The misfit of the largely coherent nitride precipitates with the surrounding ferrite matrix is strongly anisotropic. As a consequence, the nitride precipitates develop as platelets (length ≤ 30 nm and thickness ≤ 3 nm) obeying a Bain orientation relationship with the ferrite matrix with $\{100\}_{\alpha\text{-Fe}}$ habit planes, and they are surrounded by a tetragonally distorted ferrite matrix. As a result, cubic and tetragonal ferrite reflections can be discerned in both X-ray diffraction and selected area electron diffraction patterns.
3. The lattice parameter of the mixed $\text{Ti}_{1-x}\text{Cr}_x\text{N}$ nitride increases with an increasing Ti/Cr atomic ratio. Consequently, the misfit-strain field is most pronounced for the highest relative Ti content of the alloy, which corresponds with a microhardness increasing with increasing Ti/Cr atomic ratio.
4. The amount of excess nitrogen dissolved in the ferrite matrix $[\text{N}]_{\text{strain}}$ increases with increasing Ti/Cr atomic ratio as a consequence of a tensile hydrostatic component of misfit stress, which increases with an increasing Ti/Cr atomic ratio.
5. The amount of excess nitrogen adsorbed at the nitride-platelet faces, $[\text{N}]_{\text{interface}}$, increases with an increasing Ti/Cr atomic ratio because (1) Ti has a much larger affinity for N than Cr and (2) the relative amount of interfacial (nitride/matrix) area increases with an increasing Ti/Cr atomic ratio.

ACKNOWLEDGMENTS

The authors thank Dr. A. Leineweber for discussion on diffraction-profile fitting, Dipl. Ing. P. Kress and Mr. J. Koehler (Deceased on 19.07.2011) for assistance with the nitriding experiments, Mr. W. D. Lang for TEM foil preparation, and Ms. S. Haug for assistance with the EPMA measurements.

REFERENCES

1. S. Lampman: *Introduction to Surface Hardening of Steel*, ASM Handbook, vol. 4, Heat Treating, ASM International, Metals Park, OH, 1991, pp. 259–67.
2. E.J. Mittemeijer and J.T. Slycke: *Surf. Eng.*, 1996, vol. 12, pp. 152–62.
3. E.J. Mittemeijer and M.A.J. Somers: *Surf. Eng.*, 1997, vol. 13, pp. 483–97.
4. E.J. Mittemeijer: *J. Metal.*, 1985, vol. 37, pp. 16–20.
5. E.J. Mittemeijer: *Mater. Sci. Forum*, 1992, vols. 102–104, pp. 223–28.
6. P.M. Hekker, H.C.F. Rozendaal, and E.J. Mittemeijer: *J. Mater. Sci.*, 1985, vol. 20, pp. 718–29.
7. R.E. Schacherl, P.C.J. Graat, and E.J. Mittemeijer: *Z. Metallkd.*, 2002, vol. 93, pp. 468–77.
8. R.E. Schacherl, P.C.J. Graat, and E.J. Mittemeijer: *Metall. Mater. Trans. A*, 2004, vol. 35A, pp. 3387–98.

9. B. Mortimer, P. Grieveson, and K.H. Jack: *Scand. J. Metals*, 1972, vol. 1, pp. 203–09.
10. S.S. Hosmani, R.E. Schacherl, and E.J. Mittemeijer: *Mater. Sci. Technol.*, 2005, vol. 21, pp. 113–24.
11. S.S. Hosmani, R.E. Schacherl, and E.J. Mittemeijer: *J. Mater. Sci.*, 2008, vol. 43, pp. 2618–24.
12. M.H. Biglari, C.M. Brakman, E.J. Mittemeijer, and S. van der Zwaag: *Phil. Mag. A*, 1995, vol. 72, pp. 931–47.
13. M.H. Biglari, C.M. Brakman, M.A.J. Somers, W.G. Sloof, E.J. Mittemeijer, and S. van der Zwaag: *Z. Metallkd.*, 1993, vol. 84, pp. 124–31.
14. M.H. Biglari, C.M. Brakman, E.J. Mittemeijer, and S. van der Zwaag: *Phil. Mag. A*, 1995, vol. 72, pp. 1281–99.
15. M.H. Biglari, C.M. Brakman, E.J. Mittemeijer, and S. van der Zwaag: *Metal. Mater. Trans. A*, 1995, vol. 26A, pp. 765–76.
16. W.D. Welch and S.H. Carpenter: *Acta Metall.*, 1973, vol. 21, pp. 1169–79.
17. A. Krawitz: *Scripta Metall.*, 1977, vol. 11, pp. 117–22.
18. S.S. Hosmani, R.E. Schacherl, and E.J. Mittemeijer: *Acta Mater.*, 2005, vol. 53, pp. 2069–79.
19. S.S. Hosmani, R.E. Schacherl, and E.J. Mittemeijer: *Acta Mater.*, 2006, vol. 54, pp. 2783–92.
20. D.H. Kirkwood, O.E. Atasoy, and S.R. Keown: *Metals. Sci.*, 1974, vol. 8, pp. 49–55.
21. H.H. Podgurski and F.N. Davis: *Acta Metall.*, 1981, vol. 29, pp. 1–9.
22. D.S. Rickerby, S. Henderson, A. Hendry, and K.H. Jack: *Acta Metall.*, 1986, vol. 34, pp. 1687–99.
23. D.H. Jack: *Acta Metall.*, 1976, vol. 24, pp. 137–46.
24. H. Hasegawa, A. Kimura, and T. Suzuki: *J. Vac. Sci. Technol. A*, 2000, vol. 18, pp. 1038–40.
25. S.M. Aouadi, J.A. Chladek, F. Namavar, N. Finnegan, and S.L. Rohde: *J. Vac. Sci. Technol. B*, 2002, vol. 20, pp. 1967–73.
26. M.A. Baker, T.P. Mollart, P.N. Gibson, and W. Gissler: *J. Vac. Sci. Technol. A*, 1997, vol. 15, pp. 284–91.
27. J. Vetter, H.J. Scholl, and O. Knotek: *Surf. Coat. Technol.*, 1995, vol. 74–5, pp. 286–91.
28. T. Suzuki, D. Huang, and Y. Ikuhara: *Surf. Coat. Technol.*, 1998, vol. 107, pp. 41–47.
29. E.C. Bain: *Trans. AIME*, 1924, vol. 70, pp. 25–46.
30. V.A. Phillips and A.U. Seybolt: *Trans. TMS-AIME*, 1968, vol. 242, pp. 2415–22.
31. M.A.J. Somers, R.M. Lankreijer, and E.J. Mittemeijer: *Phil. Mag. A*, 1989, vol. 59, pp. 353–78.
32. E. Lehrer: *Z. Elektrochem.*, 1930, vol. 36, pp. 383–92.
33. R. Hoffmann, E.J. Mittemeijer, and M.A.J. Somers: *HTM 51*, 1996, pp. 162–69.
34. R. Delhez and E.J. Mittemeijer: *J. Appl. Cryst.*, 1975, vol. 8, pp. 609–11.
35. J.L. Pouchou and F. Pichoir: *Rech. Aerosp.*, 1984, pp. 167–192.
36. A. Armigliato, L. Dori, A. Garulli, and P. Venturi: *J. Microsc. Spectrosc. Electron.*, 1982, vol. 7, pp. 593–603.
37. N.E. Vives Diaz, S.S. Hosmani, R.E. Schacherl, and E.J. Mittemeijer: *Acta Mater.*, 2008, vol. 56, pp. 4137–49.
38. A.R. Clauss, E. Bischoff, R.E. Schacherl, and E.J. Mittemeijer: *Metall. Mater. Trans. A*, 2009, vol. 40A, pp. 1923–34.
39. Y. Massiani, P. Gravier, L. Fedrizzi, and F. Marchetti: *Thin Solid Films*, 1995, vol. 261, pp. 202–08.
40. P. Hones, R. Sanjinés, and F. Lévy: *Thin Solid Films*, 1998, vol. 332, pp. 240–46.
41. H.H. Podgurski and H.H. Knechtel: *Trans. TMS-AIME*, 1969, vol. 245, pp. 1595–1602.
42. M. Nikolussi, A. Leineweber, and E.J. Mittemeijer: *Phil. Mag.*, 2010, vol. 90, pp. 1105–22.
43. K.S. Jung, R.E. Schacherl, E. Bischoff, and E.J. Mittemeijer: *Surf. Coat. Technol.*, 2010, vol. 204, pp. 1942–46.